CHEMICAL ENGINEERING TRANSACTIONS
VOL. 54, 2016
A publication of AIDIC
The Italian Association of Chemical Engineering
Online at www.aidic.it/cet
Guest Editors: Selena Sironi, Laura Capelli

ISBN 978-88-95608-45-7; **ISSN** 2283-9216
DOI: 10.3303/CET1654009

Comparison of Tin Dioxide Ozone Sensor Operated in On/Off Switching Temperature Cycles and at Constant Temperature

Manuel Aleixandre*[a], Maria del Carmen Horrillo[a], Michel Gerboles[b], Laurent Spinelle[b], Fausto Bonavitacola[c]

[a] Grupo de I+D en Sensores de Gases, ITEFI, CSIC. Madrid, Spain
[b] European Commission, Joint Research Centre (JRC), Institute for Environment and Sustainability (IES), Ispra, Italy
[c] Phoenix Sistemi & Automazione s.a.g.l., Muralto (TI), Switzerland
manuel.aleixandre@csic.es

Commercial ozone (O_3) sensors were calibrated at the Institute for Environment and Sustainability of the Joint Research Center in Ispra (Italy). The sensors were exposed to ozone at different concentrations, ranging from 0 ppb to 110 ppb, in a climatic chamber under controlled conditions. The actual ozone concentration was not calculated from the gas control system but it was measured with standard reference methods. Some sensors were operated at constant heating power and one sensor was operated by switching on and off the power every 30 seconds. This allowed the extraction of different response curve features such as the slope of the resistance curve during the power cycle, the final resistance after that power cycle, or the difference between initial and final resistance after a power cycle. The measurement chamber was used to control different ambient parameters that could affect the sensor response such as temperature and relative humidity. All these different features and ambient parameters were combined and used in the calibration. Several models with different parameters were compared and the best one was selected. In addition to the calibration several characteristic sensor parameters were measured or calculated: hysteresis, drift, interference with different gases introduced in the chamber together with ozone: NO_2, NO, CO, NH_3. The performance of the sensors operated at constant heating power and the sensor operated by heating power switching on/off were compared.

1. Introduction

The measurement of the air quality is an important problem and cheap sensor platforms based on small commercial gas sensors are being developed worldwide (Kumar et al. 2015). The evaluation of the performance of the sensors is a necessity and there are several works related to it, theory (Aleixandre et al., 2014) or experimental (Spinelle et al. 2015). This paper presents the results of the evaluation of an ozone low-cost sensor for monitoring ambient air quality. The sensor consisted of a tin dioxide (SnO_2) thin layer placed on top of a heating resistance. The tin dioxide sensor is usually operated at constant heater power causing temperatures about 430 °C. At constant temperature mode, SnO_2 sensors show a large dependency with temperature (Wang et al. 2008) and humidity (Korotcenkov et al. 2007). The temperature dependence is generally corrected using the Arrhenius relation, see Eq (1), where σ_0 is the pre exponential factor, E_a is the activation energy of the sample, k is the Boltzman constant and T is the absolute temperature. Conversely, humidity effects on SnO_2 sensors are rarely corrected for.

$$\sigma = \sigma_0 \, exp(-Ea/kT) \quad (1)$$

On the other hand, (Losch et al. 2008), showed that using a SnO_2 sensor, O_3 can be determined in the range from 0 to 100 ppb with sensor Temperature Cycle Operation (TCO). The authors used a pattern of temperature varying linearly between ambient temperature and about 400 °C every 30 s. This mode of operation was shown to improve stability and reduce cross sensitivity to typical interfering gases compared to constant temperature operation. The authors showed that the feature extraction (the slope and 2nd derivative of the resistance curve during power cycles, the initial and final resistance of each power cycle, and the

Please cite this article as: Aleixandre M., Horrillo C., Gerboles M., Spinelle L., Bonavitacola F., 2016, Comparison of tin dioxide ozone sensor operated in on/off switching temperature cycles and at constant temperature, Chemical Engineering Transactions, 54, 49-54
DOI: 10.3303/CET1654009

difference between initial and final resistance after a power cycle) and concentration prediction algorithm considerably improves reproducibility, yielding valid results also for aged sensors and even when applied to different sensors of the same type reducing the necessity of individual sensor calibration. In the same way as for TCO, more information may be drawn from SnO_2 sensors by switching on and off the power of the heater every 30 seconds instead of operating the sensor with a constant power. In this paper, the performances of SnO_2 ozone sensors under the two modes of operation, constant power and On/Off Switching Operation mode (OFSO), are compared.
In the following, the set of different features and ambient parameters were combined and used in the calibration. Several models with different parameters were compared and the best one was selected. In addition to the calibration several characteristic sensor parameters were measured or calculated: hysteresis, drift, interference with different gases introduced in the chamber simultaneously to the ozone exposure: NO_2, NO, CO, NH_3 (Spinelle et al. 2013). The results were validated by a subset of measurements and evaluated by different parameters. The integration of additional parameters improved the calibration results. Experiments were carried out in an exposure chamber under controlled conditions in order to calibrate the sensor, determine metrological characteristics and evaluate the effect of temperature, humidity, and cross sensitivities with gaseous interfering compounds.

2. Experimental setup

In this study, the MiCS-Oz-47 (SGX-Sensortech-CH) gas sensors were tested for monitoring O_3 in ambient air. The Oz-47 is a microprocessor based Printed Circuit Board module designed for ozone sensing applications. It accommodates a dual ozone gas sensor (MiCS 4614), a temperature sensor and a relative humidity sensor. The gas sensor is a micro-machined silicon structure equipped with a sensitive resistance R_S placed on top of a heating resistance R_h. The sensitive element is a tin dioxide (SnO_2) thin layer. The sensor operated at constant heater power, P_h of 80 mW, causes the temperature of R_S to reach about 430 °C. A LabView software was designed to control the heater of the OZ-47 software and to acquire temperature, humidity and resistance values. A set of 8 sensors was controlled using one serial communication line multiplexed through the COM port on a PC running the LabView software. One of these Oz-47 sensors underwent OFSO every 30 s by sending LabView commands through the same channel. Data acquisition was carried out recording the measurements of resistance, temperature and humidity at the higher possible frequency of the PCB (1Hz). The measurements of the sensors operated at constant temperature were minute averaged. The sensors were not calibrated by the manufacturers. They were installed inside the JRC laboratory exposure chamber for evaluation. The exposure chamber is described elsewhere (Spinelle, Gerboles, Aleixandre, 2014). This chamber is able to generate gaseous mixtures and to control humidity, temperature and wind velocity. All parameters are automatically and independently measured set and controlled. It can accommodate several sensors for simultaneous testing with an internal volume of about 120 L. The reference values of all compounds are measured allowing the full traceability to national/international units when evaluating sensors. The ozone sensors were enclosed into a polyamide (PA66GF30) housing and O_3 molecules had to diffuse through a PTFE membrane to reach the SnO_2 sensitive layer.
Two MicroCal 5000 (Umwelttechnik MCZ Gmbh) generators were used for generating O_3. These generators are equipped with current intensity regulated UV lamps placed in thermos-insulated chamber. Prior to experiment, Mass Flow Controllers (MFC) used for the gas mixture generation were calibrated against a Primary Flow Calibrator Gilian Gilibrator-2. A 10 L/min MFC for dry air and a 10 L/min MFC for humid air were used for filling the chamber excepted for the response time experiment. Seen the internal volume of the exposure chamber (about 120 L), it was decided to use the 100 L/min automatic bench that JRC uses for the European inter-comparison exercises of the National Reference Laboratories of Air Pollution (Barbiere, et al., 2011) for this test to reach stability in less than 2 minutes in the exposure chamber. Reference methods were used for monitoring O_3 (Thermo Environment TEI 49C UV-photometer), $NO/NO_x/NO_2$ (Thermo Environment 42 C chemiluminescence analyser), SO_2 (Environment SA AF 21 M flourescent analyser), CO (Thermo Environment 48i-TLE NDIR analyser) and NH_3 (Thermo Environment Model 17i, courtesy of monitoring network of Bolzano/Bozen – Italy). For CO_2, an infrared sensor, Gascard NG 0-1000 µmol/mol (Edinburg Sensors – UK) was used. The gaseous interfering compounds were generated either using a dynamic dilution of highly concentrated cylinders or using an in-house developed permeation system able to accommodate 8 permeation cells whose sweep flows about 200 mL/min were controlled with critical orifices (Calibrage SA). Each permeation cell was dipped in a water bath consisted (Haake W26 Thermostatic Circulating Water Bath with Haake E8 Controller). The temperature of each cell was set at 40 °C. The permeation tubes were weighed every three weeks. The permeation cells were filled with NO_2, SO_2, NH_3 and HNO_3 permeation tubes manufactured by KinTec and Calibrage. CO mixtures were directly generated by dynamic dilution from highly concentrated cylinders from Air Liquide.

3. Results

The Figure 1 shows the response curve of one of this power cycles with some of the features extracted from the curve. Those features were: the slope of a fitted line to the sensor response ramp during the power cycle (Slope), the resistance at the end and at the start of the power cycle (R_{ini}, R_{end}), the Pearson regression coefficient for the fitted curve (R2). Also we used two transformation features: Slope/R2 and R_{end}/R2. After extraction, the features were filtered by a Savitzky-Golay filter of order 1 and a window size of 51 points. Figure 1 shows the extracted feature Slope along several O_3 steps. Each point represents a measurement and the filtered curve is represented as a red line over it.

3.1 Response time

The response time of sensors (t_{90}) was computed by averaging the time needed by the sensor to reach 90 ppb from 0 ppb ($t_{0\text{-}90}$) and the time needed to reach zero starting at 90 ppb ($t_{90\text{-}0}$). During these tests the temperature, humidity and the possible interfering gas compounds were kept constant. Table 1 shows the response times of the sensors. The response time remained within half an hour with similar rise time and lag time for the constant power operated sensors. For the power cycled sensor the response time increased five times up to 142 minutes.

3.2 Calibration

The calibration of O_3 concentration levels included 90, 40, 0, 60, 20, 110 ppb in randomized order to take into account any possible hysteresis effect. For the sensor operated under constant power a saturation phenomena of the response of SnO_2 sensors versus O_3 at high concentration levels (Lösch et al. 2008) was observed. Several models were fitted address this saturation effect: Michelis Munten Eq. (2), Hill equation Eq. (3), exponential decay of increasing form Eq. (4), and polynoms of 2nd and 3rd order (Kurganov et al. 2001) where R is the sensor response at any O_3 level, R_{max} the maximum sensor response, $O_{3,Rmax/2}$ is the O_3 level at half of R_{max}, h is the slope at $O_{3,Rmax/2}$, C is the sensor response at 0, a is the response increase between C and Rmax and K is $1/O_{3,Rmax/2}$.

$$R = R_{max} O_3 / (O_{3,Rmax/2} + O_3) + C \quad (2)$$

$$R = R_{max} O_{3,Rmax/2}^{h} / \left(O_{3,Rmax/2} + O_3\right)^{h} + C \quad (3)$$

$$R = a(1 - e^{-KO_3}) + C \quad (4)$$

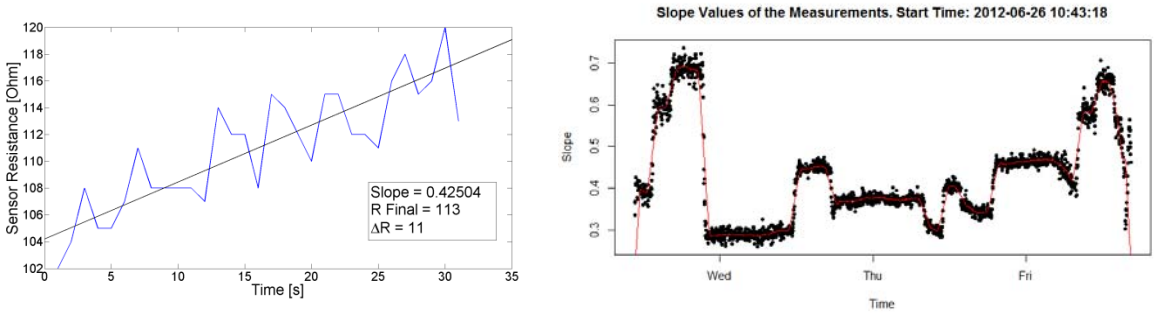

Figure 1: Example of sensor response along a heating power cycle (left). Plot of slopes extracted each minute (black dots) along a profile of several O_3 steps and the filtered feature (slopes) as a red line (right)

The Akaike information criterion (Sakamoto et al. 1986) was used to estimate the information lost with each model when representing the calibration data and to balance the goodness of fit of the models with their complexity shown by the number of parameters to be estimated. For 6 sensors out of 7 the most empirical model, the polynom of 3rd order, gave the lowest AIC value while for the last one a parabolic model was found best. For the sensor operated with OFSO cycles we used several set of features and compared the uncertainty, the best one was the first discrimination function (DF1) of a Linear Discriminant Analysis (LDA). An example of calibration can be seen in Figure 2 for both operative mode and the Table 2 shows the lack of fit and residuals.

Table 1: Sensor's response time of sensors evaluated in the exposure chamber. Calibration data with the standard uncertainty of lack of fit u(lof), the maximum and standard deviation (s) of residuals. Results are given for the constant power operation (average of 7 sensors results) and one sensor with OFSO *operation*

Sensors	t_{90} [min]	$t_{0\text{-}90}$ [min]	$t_{90\text{-}0}$ [min]	Lack of fit [ppb]	Max residual [ppb]	s of residual [ppb]
Constant power (n=7)	29 ± 13	28 ± 13	30 ± 13	4.9 (± 2.9)	7.9 (±5.5)	4.4 (3.1)
On/Off cycles	143	167	119	10	15	9.2

3.3 Repeatability and limit of detection

The repeatability and the limit of detection of the sensors (see Table 2) were estimated by calculating the standard deviation of 3 successive sensor values, sr, with the sensor measuring at 0 and at about 90 ppb while other exposure conditions were kept constant. The repeatability of sensor was computed as $2\sqrt{2}$ sr (sr at 90 ppb) and the limit of detection was estimated as 3sr (sr at 0 ppb).

3.4 Sensor drift

For the short term drift, sensor responses were evaluated at 0, 60 and 90 ppb of O_3 on three consecutive days, each of them being separated by a period of time between 12 and 36 hours. The mean deviations of the sensor responses over days, Dss, were calculated. The contribution to the measurement uncertainty u(Dss) was calculated using a quadratic sum of Dss and a pooled standard deviation of the Dss at all concentration levels (Table 2). The Figure 3 shows the long term drift of one sensor operated at constant power and the sensor operated in OFSO cycles. It can be seen that after 70 days of constant power cycles the response of the sensor deteriorates and the sensitivity to the ozone concentrations decreases.

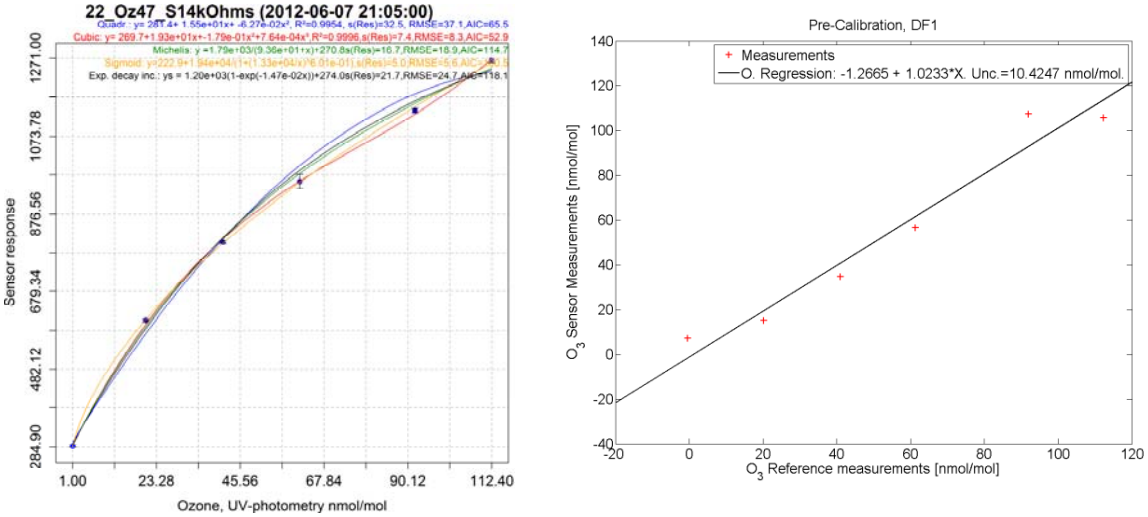

Figure 2: Example of calibration of OZ-47 using constant temperature (left) and on/off cycle operations (right)

Table 2: Standard deviation at 0 and 90 ppb, limit of detections (lod) and repeatability at 90 ppb (r) for minute values. The four columns on the right gives the drift (Dss) and its standard uncertainty u(Dss)

Sensors	s_r 0/ s_r 90 (ppb)	lod (pbb)	R at 90 ppb(ppb)	Dss (ppb)	u(Dss) (ppb)
Constant power (n=7)	0.3/1.7	3.7 ± 2.5	5.9 ± 7.1	3.5	4.6
On/Off cycles	9.7/ 11.4	29	16	10	26

3.5 Gaseous interfering compounds

The effect of NO_2 for O_3 sensors, together with the effect of NO, CO, CO_2 and NH_3 were evaluated at two levels. The influence of each interfering compound was determined separately. The tests were carried out at 22°C and 60 % of relative humidity and in absence of other interfering compounds. For each compound, we determined the sensitivity coefficient b and the difference of sensor responses divided by the level of the interfering compound (see Table 3).

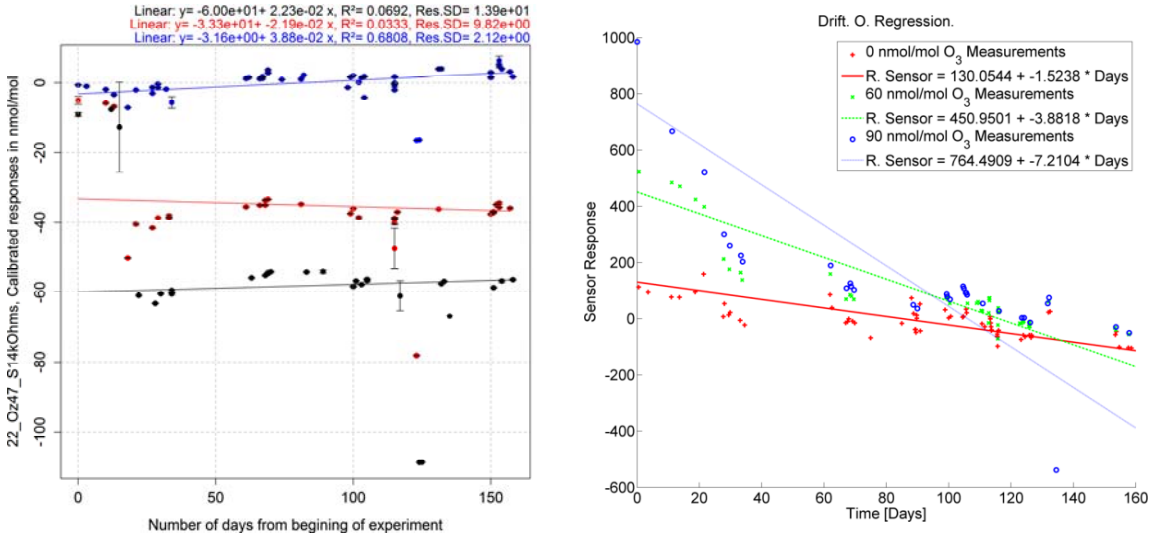

Figure 3: Plot of the long term drift at constant temperature (left) and on/off cycle operation (right)

Table 3: Gaseous interfering compounds: sensitivity coefficients ± standard uncertainty in ppb. For temperature and humidity: sensitivity coefficients / standard uncertainty in ppb

Sensors	NO_2 [ppb/ppb]	NO [ppb/ppb]	CO [ppb/ppm]	CO_2 [ppb/ppm]	NH_3 [ppb/ppb]	Temperature [ppb/ºC]	Humidity [ppb/%Hd]
Constant power (n=7)	0.04 ± 0.04	-0.031±0.014	-0.01±0.0026	0.226±0.0679	0.004±0.006	-2.61 ± 2.56	-0.94/0.30
On/Off cycles	1.01	0.19	1.39	-	-	-0.7	8.8

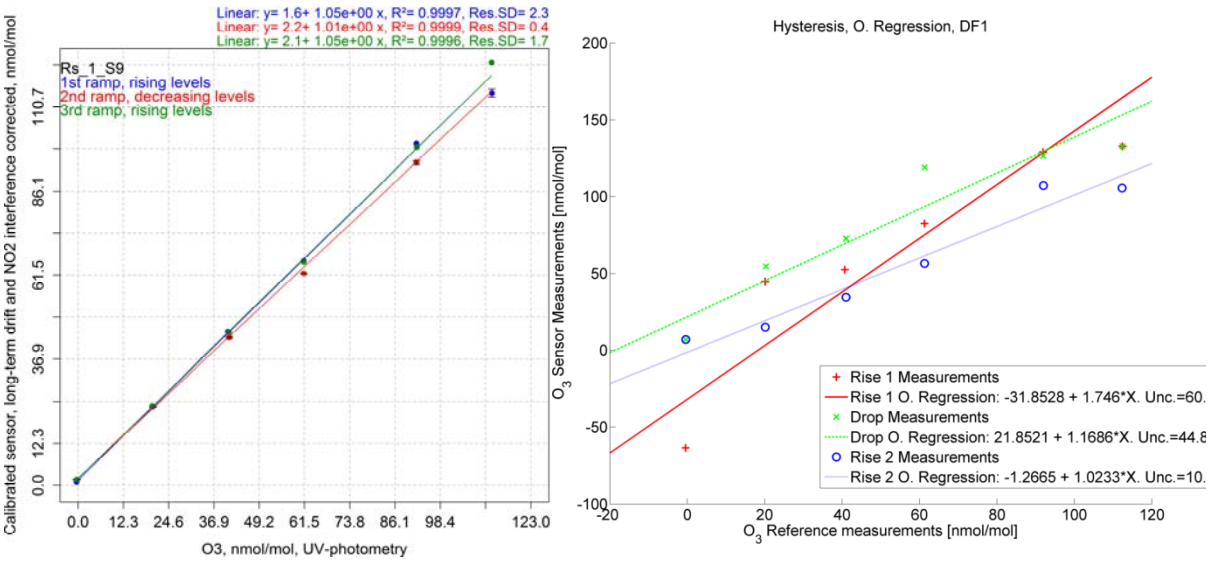

Figure 4: Plot of the Oz-47 hysteresis effect for the constant temperature (left) and OFSO operation (right)

3.6 Temperature and humidity effects

The sensor responses were influenced by changes of temperature and relative humidity. Two series of tests were conducted independently generating ramps of temperature and humidity in a hysteresis cycle while gaseous levels in the chamber were kept constant. The ranges of temperature changed between 12 and 32 ºC (by step of 5 ºC) and the range of humidity was kept between 40% and 80% (by step of 10%). The results of the tests are given in Table 3, including sensitivity coefficients of the sensors to temperature and

humidity. The standard uncertainties include both the contribution from the sensitivity coefficients and hysteresis effect.

3.7 Hysteresis

Finally the estimation of the dependence of sensors toward hysteresis was carried out using the calibration levels with a ramp of rising O_3 levels followed with a ramp of decreasing levels and finally with another rising ramp. Three calibration lines were plotted, one for the 1st ramp of rising levels, one for the falling levels and one for the 2nd ramp of rising levels. For the constant temperature operation, the results changed from sensor to sensor (n=7). 4 sensors presented differences within 10 % for the 3 ramps while 2 of them had differences slightly over 10 % and one sensor had differences of slopes of about 30 %. The hysteresis of the sensor operated in power cycles was higher reaching up to 60% of increase in the slope as seen in Figure 4.

4. Conclusions

The uncertainty of the MiCS-Oz-47 sensors operated at constant power is 4.9 ppb and it is doubled by using the power cycle operation and also other parameters, as the limit of detection or repeatability of the measurements, greatly decrease. The OFSO operation provides sensor information that can be used for measurement of ozone concentration. However, the uncertainty of the calibration increases compared to the uncertainty of the constant heating power operated sensor. Due to this increased sensor variability, the uncertainty caused by all the parameters (humidity, hysteresis, gas interferences) increases. Finally, a drastic long term drift and possible saturation of the heating power cycle operated sensor is observed. The ambient temperature dependence is the only parameter that improves, the temperature sensitivity of the cycle power sensor decreases 3.7 times in this case. In general, the incorporation of additional parameters improved the calibration results, lowering the uncertainty. Compared to the on/off operation, constant powered sensors gave more suitable results. It is likely that the simple on/off operation is not able to provide sufficient information compared to a more elaborate temperature pattern that was shown to improve the stability and reduce cross sensitivities which are the main drawbacks of MOx sensors (Lösch et al.,2008).

Acknowledgments

This study was carried out within the EMRP Joint Research Project ENV01 MACPoll. The EMRP is jointly funded by the EMRP participating countries within EURAMET and the European Union.

References

Aleixandre M., Gerboles M., 2012, Review of Small Commercial Sensors for Indicative Monitoring of Ambient Gas. Chemical Engineering Transactions 30, 169–74. doi:10.3303/CET1230029.

Barbiere M., Stummer V., Lagler F., Mücke HG., 2011, Evaluation of the Laboratory Comparison Exercise for SO_2, CO, O_3, NO and NO_2, Publications Office of the European Union, Luxembourg, doi:10.2788/33334

Kurganov B.I., Lobanov A.V., Borisov I.A., Reshetilov A.N., 2001. Criterion for Hill equation validity for description of biosensor calibration curves. Analytica Chimica Acta 427, 11–19. doi:10.1016/S0003-2670(00)01167-3.

Korotcenkov G., Blinov I., Brinzari V., Stetter J.R., 2007. Effect of air humidity on gas response of SnO2 thin film ozone sensors. Sensors and Actuators B: Chemical 122, 519–526. doi:10.1016/j.snb.2006.06.025

Kumar P., Morawska L., Martani C., Biskos G., Neophytou M., Di Sabatino S., Bell M., Norford L., Britter R., 2015, The rise of low-cost sensing for managing air pollution in cities, Environment International, Volume 75, Pages 199-205, ISSN 0160-4120, http://dx.doi.org/10.1016/j.envint.2014.11.019.

Lösch M., Baumbach M., Schütze A., 2008. Ozone detection in the ppb-range with improved stability and reduced cross sensitivity. Sensors and Actuators B: Chemical 130, 367–373. doi:10.1016/j.snb.2007.09.033

Sakamoto Y., Ishiguro M., and Kitagawa G., 1986. Akaike Information Criterion Statistics. D. Reidel Publishing Company. ISBN 9027722536

Spinelle L., Gerboles M., Aleixandre M., 2013, Protocol of evaluation and calibration of low-cost gas sensors for the monitoring of air pollution, Publications Office of the European Union, Luxembourg (Luxembourg). doi: 10.2788/9916

Spinelle L., Gerboles M., Aleixandre M., 2014, Report of laboratory and in-situ validation of micro-sensor for monitoring ambient air - Ozone micro-sensors, AlphaSense, model B4-O3 sensors (UK), EUR 26681, Publications Office of the European Union. doi:10.2788/84725

Spinelle L., Gerboles M., Aleixandre M., 2015, Performance Evaluation of Amperometric Sensors for the Monitoring of O3 and NO2 in Ambient Air at ppb Level, Procedia Eng., vol. 120, pp. 480–483, doi:10.1016/j.proeng.2015.08.676